Journal of Metals, Materials and Minerals, 36(1), e2600, 2026

A top-electrode-based liquid-solid triboelectric nanogenerator for energy harvesting and ethanol detection

Subrat BHOL[1], Nakul Charan SAHU[1], Sunit Gourav MOHANTY[2], Vicky Raj MADDALA[3], Basanta Kumar PANIGRAHI[1,*], and Premkumar BHOSALE[4,*]

[1] *Department of Electrical Engineering, Siksha O Anusandhan (deemed to be University), Bhubaneswar 751030, India*
[2] *Department of Environmental Sciences, Sambalpur University, Burla 768019, India*
[3] *Department of Physics, Andhra Loyola College, Vijayawada, 520008, India*
[4] *School of Nanoscience & Technology, Shivaji University, Kolhapur 416004, India.*

***Corresponding author e-mail**: basanta1983@gmail.com, premkumarbhosale2424@gmail.com

Received date:
12 December 2025
Revised date:
23 December 2025
Accepted date:
26 December 2025

Keywords:
Liquid-solid;
Energy harvesting;
Ethanol detection

Abstract

Liquid-solid triboelectric nanogenerators (LS-TENGs) offer a promising avenue for self-powered energy harvesting and sensing by exploiting contact electrification at fluid-dielectric interfaces, where droplet dynamics drive charge separation for electrical output without external power. In this work, a top-electrode LS-TENG was fabricated using a polytetrafluoroethylene (PTFE) film on a PMMA substrate with deionised water droplets, achieving an open-circuit voltage of –3.4 V, short-circuit current of 3.6 μA, and peak power of 1.48 nW at 100 MΩ under optimised conditions of 2 cm drop height, 45° tilt, and 50 μL volume. Performance scaled with droplet kinetics and volume due to enhanced contact area and charge transfer, while stability persisted over repeated cycles, and ethanol-water mixtures distinctly modulated outputs via reduced permittivity and wettability, enabling sensitive, battery-free detection for practical applications in environmental monitoring.

1. Introduction

Ethanol detection holds paramount importance in diverse industrial, environmental and health-related domains, where precise monitoring ensures compliance with regulatory standards, optimizes production processes and mitigates risks associated with its flammability, volatility and toxicity [1-4]. In biofuel manufacturing and blending, accurate ethanol quantification prevents phase separation in gasoline mixtures, safeguards engine performance and reduces emissions, while in the beverage and pharmaceutical sectors, it verifies product quality, labelling accuracy and formulation integrity to meet stringent safety guidelines [5-8]. Beyond these applications, ethanol sensing supports food spoilage detection, occupational safety through exposure limits, drunk driving prevention via breath analysis and environmental emission control, yet traditional methods like gas chromatography, densitometry and spectroscopy often demand sophisticated equipment, skilled operators and external power, hindering their use in portable or real-time scenarios [9-12]. Moreover, the growing demand for decentralized, on-site and continuous ethanol monitoring in smart manufacturing, wearable health diagnostics and Internet-of-Things (IoT) based environmental platforms has intensified the need for compact, low-cost and energy-efficient sensing technologies capable of operating in resource-limited environments.

LS-TENGs represent an innovative self-powered technology that harnesses contact electrification and electrostatic induction at liquid-solid interfaces to generate electrical outputs from mechanical interactions, such as liquid flow, oscillation or droplet impingement on dielectric surfaces [13-17]. These devices form an electrical double layer during interfacial contact, where charge transfer depends on liquid properties like permittivity, conductivity and surface tension, enabling simultaneous energy harvesting and sensing capabilities without external power sources [18-21]. Their self-powered functionality, structural simplicity and compatibility with flexible and miniaturized designs position LS-TENGs as attractive candidates for next-generation ethanol monitoring in portable, wearable and in situ sensing systems. In a recent study, Kaja *et al.* developed an LS-TENG using surface-modified waste textiles, delivering a power output of 45 nW at 50 MΩ. The device was further applied for the reliable detection of milk adulteration [22]. The same team designed an LS-TENG using a discarded waterproof textile, such as an old raincoat, as the solid layer and water as the liquid counterpart. The device produced output signals of 0.5 V and 4 nA. It functioned as a multisource energy harvester capable of capturing energy from both wind and falling water droplets [23]. In another study, Chaithaweep *et al.* systematically compared droplet-based triboelectric nanogenerators (DEGs) using PTFE surfaces across double, top, and bottom electrode designs, revealing that the

double-electrode setup yields superior outputs up to –70 V and 22 μA through enhanced charge dynamics and electrical double-layer effects. The device was tested for real-time acid rain sensing via distinct voltage responses to pH variations [24].

In this study, we developed an LS-TENG using polytetrafluoroethylene (PTFE) as the solid dielectric layer and deionised (DI) water as the liquid phase, operating in a top-electrode configuration. The device generated an open-circuit voltage (V_{OC}) of –3.4 V and short circuit current of (I_{SC}) of 3.6 μA , with a maximum power of 1.48 nW at an external load of 100 MΩ. Beyond its energy-harvesting capability, the LS-TENG was further employed for ethanol detection, where changes in the electrical response enabled sensitive identification of ethanol concentrations. These self-powered sensing systems highlight a promising route toward portable, battery-free analytical devices, offering a simple, more sustainable alternative to conventional instrumentation.

2. Materials and methods

2.1 Materials

PTFE film, aluminium tape, and PMMA substrate were used to develop the top electrode LS-TENG.

2.2 TENG fabrication method

The cleaned PTFE film was carefully placed on the PMMA substrate using a strip of 3M adhesive tape to ensure firm attachment and uniform contact. A thin, narrow strip of aluminium tape was then positioned on the upper surface of the PTFE layer, serving as the top electrode. The aluminium electrode was subsequently connected to the oscilloscope's positive terminal for signal measurement during operation.

2.3 Characterisation techniques

The $V_{(OC)}$ of the TENG was recorded using a digital storage oscilloscope (Model DSOX1202A, Keysight, USA) equipped with a 10 MΩ high-impedance probe. The short-circuit current ($I_{(SC)}$) output was acquired through a preamplifier circuit employing an LMC-6001 operational amplifier with a 10 kΩ feedback resistor. To evaluate the electrical performance under different load conditions, the output voltage signals were monitored using a Keithley 6514 electrometer interfaced with LabVIEW software for data acquisition and analysis. The surface morphological characteristics were analyzed by scanning electron microscopy (SEM) using a Hitachi SU-8020 system/

3. Results and discussion

The digital and schematic representations of the fabricated LS-TENG are presented in Figure 1(a-b), respectively. The $V_{(OC)}$ and ($I_{(SC)}$) of the LS-TENG were measured with the substrate positioned at a 45° inclination, while the water droplet was released from a height of 2 cm. Figure 1(c) shows the surface morphology of the PTFE. As illustrated in Figure 1(d-e), the device exhibited a $V_{(OC)}$ of –3.4 V and an ($I_{(SC)}$) of 3.6 μA under these operating conditions. Figure 2 illustrates the working mechanism of LS-TENG. A falling water droplet first approaches the negatively charged solid tribolayer surface, where interfacial interaction initiates the build-up of an electric double layer, accompanied by tribo-electric charge separation, as the droplet begins to spread (Figure 2(a-b)). During spreading, the droplet injects additional negative charges onto the solid tribolayer while retaining net positive charges. Once its contact area extends to the nearby single electrode, the droplet forms a conductive bridge that electrically couples the solid surface and electrode into one continuous system, thereby breaking the initial electrostatic equilibrium and driving charge flow between the electrode and ground (Figure 2(c)). As the droplet subsequently shrinks and detaches, this liquid bridge is removed, partial charge neutralization occurs on the tribolayer, the induced charges at the electrode relax back toward ground, and the system returns to a new equilibrium state upon arrival of the next droplet, the sequence of spreading, bridging, charge redistribution, and separation (Figure 2 (a-d) repeats, enabling continuous power generation while effectively harvesting triboelectric charges at the liquid-solid interface.

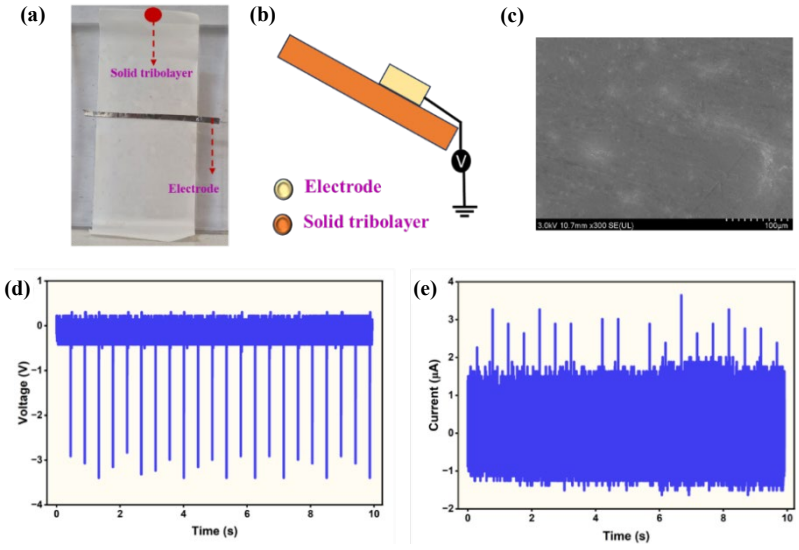

Figure 1. (a, b) Digital and schematic images of fabricated LS-TENG, (c) surface morphology of PTFE, (d) open-circuit voltage, and (d) short-circuit current of LS-TENG.

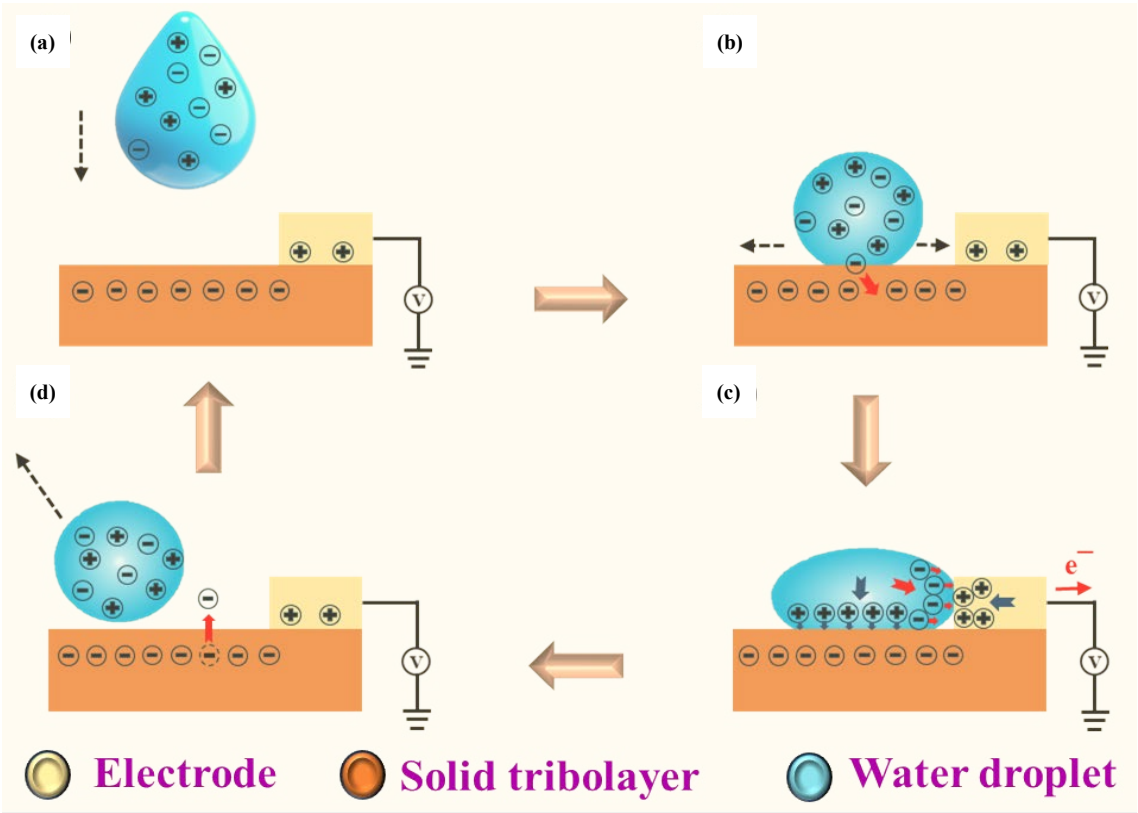

Figure 2. Working mechanism of LS-TENG.

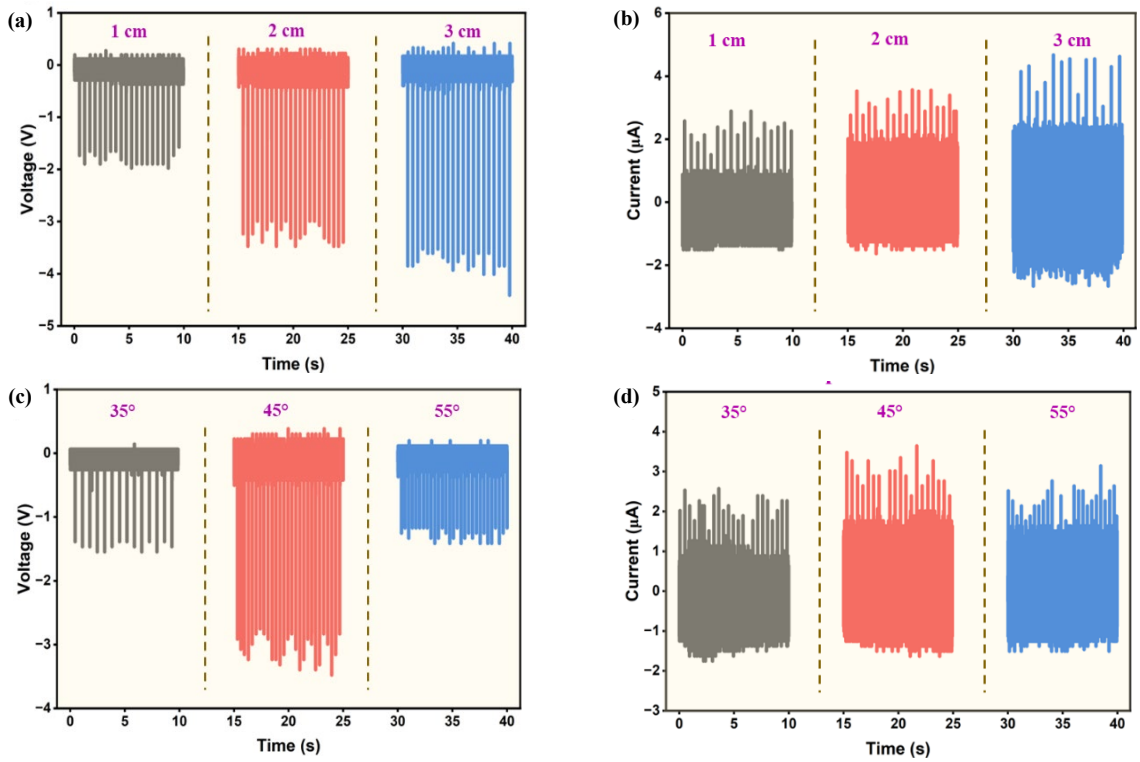

Figure 3. (a, b) open-circuit voltage and short-circuit current at various drop heights at a fixed angle of 45°, (c, d) open-circuit voltage and short-circuit current at different substrate angles at a constant drop height of 2 cm.

Figure 3(a-b) presents the $V_{(OC)}$ and short-circuit current $I_{(SC)}$ for droplet falling heights of 1 cm, 2 cm, and 3 cm. With increasing droplet height, both $V_{(OC)}$ and $I_{(SC)}$ rise, which is attributed to the greater kinetic energy of the droplet leading to a larger effective contact area with the PTFE surface and thus more efficient electron transfer during impact. Figure 3(c-d) illustrate the effect of substrate tilt angle in the range of

35° to 55°. At a tilt angle of 45°, the device exhibits the highest electrical output, owing to the increased charge density associated with the higher contact velocity and the enhanced sliding motion of the droplet along the PTFE surface. Tilting the device to 45° also promotes rapid droplet transport, effectively shortening the electron transport time through the external circuit and thereby improving the overall electrical performance. Figure 4(a-b) illustrate the influence of droplet volume on the electrical output of the LS-TENG under fixed operating conditions, with the droplet height maintained at 2 cm and the substrate tilt angle set to 45°. As the droplet volume increases from 50 µL/drop to 80 µL/drop, the $V_{(OC)}$ rises from approximately –3.4 V to –6.4 V, while the $I_{(SC)}$ increases from about 3.6 µA to 4.98 µA, which is attributed to the enlarged spreading area of the droplet on the PTFE surface that enhances charge transfer. Figure 4(c) demonstrates that the LS-TENG delivers a nearly constant voltage output over different frequencies (0.6 Hz and 2.4 Hz), indicating that the triboelectric response is governed predominantly by the relative contact area and interfacial interaction between the liquid and solid rather than by the droplet impact speed; consequently, variations in water-drop velocity exert a negligible influence on the output signals. Figure 4(d) confirms the operational stability of the LS-TENG under fixed conditions, a droplet height of 2 cm and a substrate tilt angle of 45°, where the device performed a consistent voltage profile over an extended period. Figure 4(e) demonstrates the stability of the device up to 14 day. Figure 4(f) shows the electrical output of the LS- TENG under liquid droplets with different pH values. At acidic conditions (pH 3), the droplet contains a high concentration of H^+ ions, while under alkaline conditions (pH 11), OH^- ions are dominant. The excess of either ionic species alters the interfacial charge distribution and increases the ionic strength at the liquid-solid interface, which weakens effective surface charge accumulation and results in a diminished electrical response. In contrast, at neutral condition (pH 7), the balanced presence of H^+ and OH^- ions maintain stable interfacial electrostatic conditions, enabling comparatively enhanced and consistent electrical output.

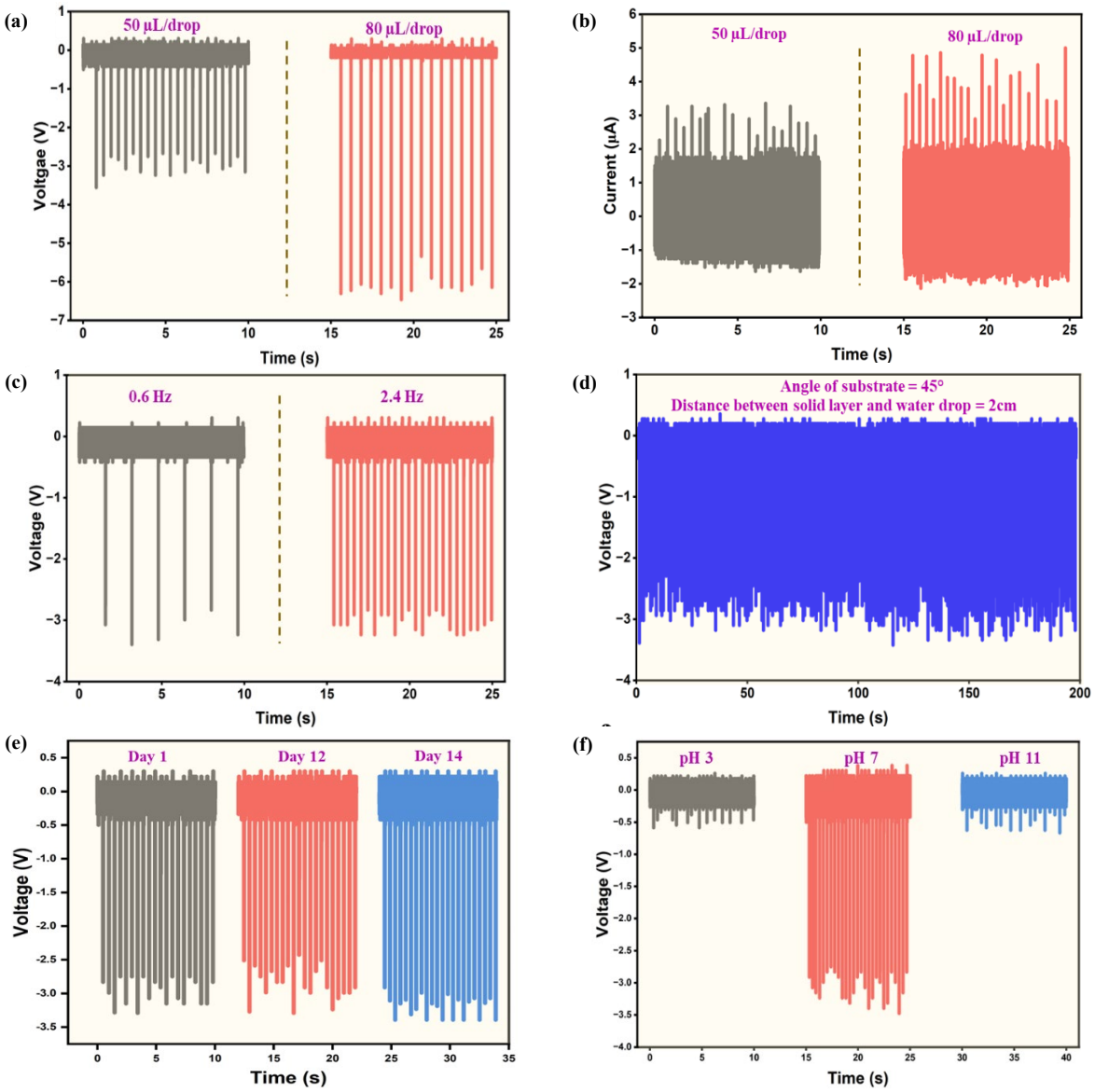

Figure 4. (a) open-circuit voltage, (b) short-circuit current responses for different water droplet volumes, (c) open-circuit voltage response at different droplet frequencies, (d) long-term stability of the LS-TENG measured at a substrate angle of 45° and a fixed drop height of 2 cm, (e) long term stability of the device upto 14 day, and (f) open-circuit voltage response at different pH.

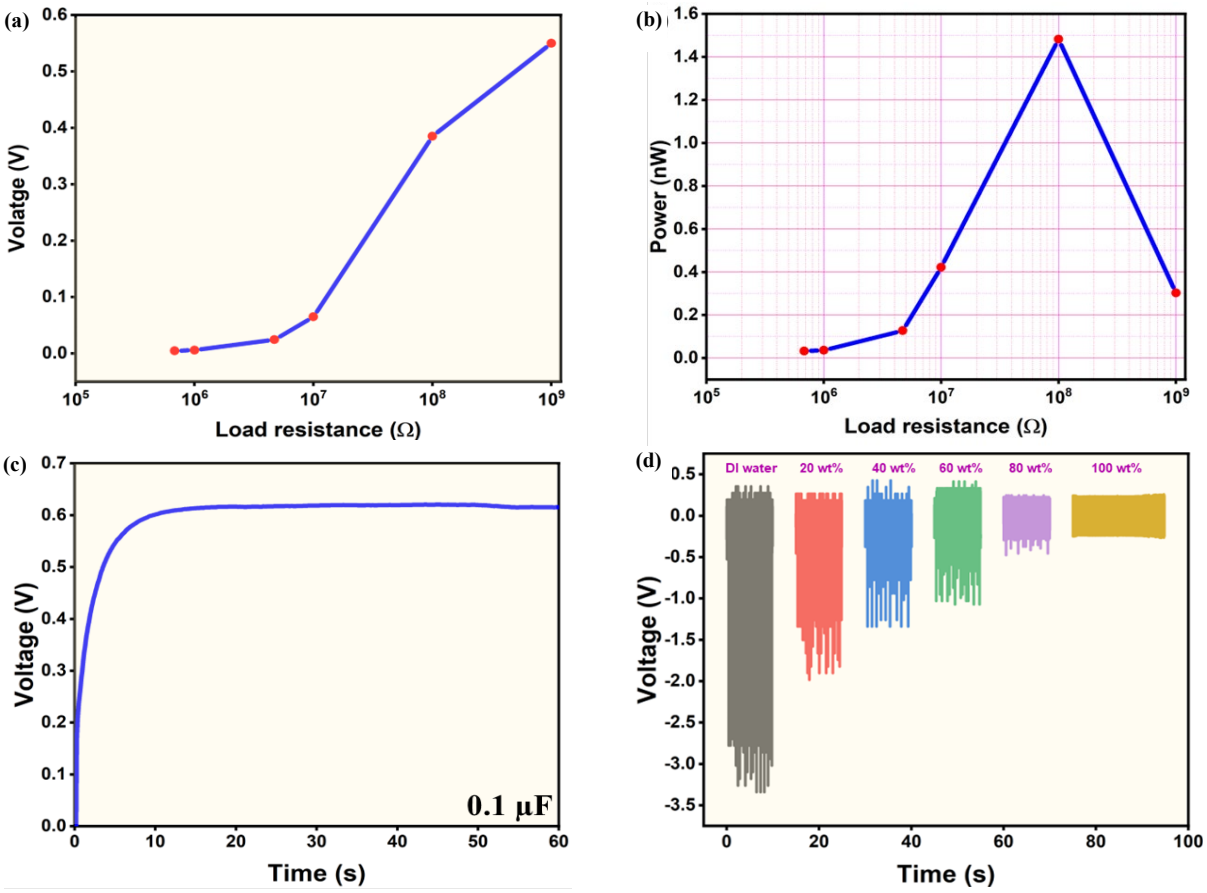

Figure 5. Electrical response of LS-TENG (a) voltage across various resistances, (b) calculated power, (c) charging of 0.1 μF capacitor, and (d) open-circuit voltage response for different ethanol-water mixtures.

Figure 5(a-b) present the output characteristics of the LS-TENG under different external load resistances. As the load resistance increases, the output voltage rises accordingly, reflecting the Ohmic dependence of voltage on resistance and indicating that larger resistances impose a greater impedance to charge transport in the external circuit. Under these conditions, the LS-TENG delivers a maximum output power of approximately 1.48 nW at an optimal load of 100 MΩ. Figure 5(c) depicts the charging behaviour of a 0.1 μF capacitor driven by the LS-TENG, where the voltage across the capacitor rapidly increases and then gradually saturates, demonstrating the capability of the device to accumulate and store the harvested energy for subsequent use. Figure 5(d) examines the effect of ethanol addition on the electrical output of the LS-TENG by using ethanol–water mixtures with 20 wt%, 40 wt%, 60 wt%, 80 wt%, and 100 wt% ethanol, while the total solution volume is fixed at 50 mL in each case. As the ethanol quantity increases, the output voltage shows a clear decreasing trend. This behaviour arises because ethanol possesses a lower polarity and dielectric constant than water, so increasing its proportion in the mixture reduces the effective permittivity and weakens the interfacial electric field, thereby decreasing the triboelectric charge generated on the PTFE surface during contact. In addition, ethanol modifies the surface tension on PTFE, leading to less favourable spreading and a reduced effective contact area, which further lowers the number of active sites available for charge transfer in each droplet event. At high ethanol concentrations, the altered hydrogen-bonding network and charge transport in the liquid accelerate charge neutralisation, resulting in a further suppression of the net triboelectric potential and thus a lower electrical output.

4. Conclusion

This investigation introduces a top-electrode LS-TENG constructed from a polytetrafluoroethylene (PTFE) tribolayer paired with DI water, yielding an open-circuit voltage of –3.4 V, short-circuit current of 3.6 μA, and peak power of 1.48 nW across a 100 MΩ load. Electrical outputs arise from dynamic charge separation during droplet spreading and retraction on the hydrophobic PTFE, enabling consistent harvesting from low-volume liquid motion. Extending this platform to ethanol sensing, the device reliably distinguishes concentrations through modulated triboelectric signals tied to permittivity shifts and advancing self-sustaining detection free from external power demands.

References

[1] M. A. Belal, S. Hajra, S. Panda, K. R. Kaja, K. J. Park, R. Jana, P. G. R. Achary, and H. J. Kim, "Functionalized MWCNTs@ ZnO nanocomposites via spray printing for NO_2 gas sensing," *Journal of Materials Science: Materials in Electronics,* vol. 36, no. 12, p. 750, 2025.

[2] K. Xia, and M. Yu, "Highly robust and efficient metal-free water cup solid–liquid triboelectric nanogenerator for water wave

energy harvesting and ethanol detection," *Chemical Engineering Journal,* vol. 503, p. 157938, 2025.

[3] L. Wang, Y. Kang, X. Liu, S. Zhang, W. Huang, and S. Wang, "ZnO nanorod gas sensor for ethanol detection," *Sensors and Actuators B: Chemical,* vol. 162, no. 1, pp. 237-243, 2012.

[4] L. Pan, J. Wang, P. Wang, R. Gao, Y-C. Wang, X. Zhang, J-J. Zou, and Z. L. Wang, "Liquid-FEP-based U-tube triboelectric nanogenerator for harvesting water-wave energy," *Nano Research,* vol. 11, no. 8, pp. 4062-4073, 2018.

[5] M. A. Belal, S. Hajra, S. Panda, K. R. Kaja, A. A. E. Moneim, P. G. R. Achary, and H. J. Kim, "Mechanochemically synthesized ZIF-8@ ZnO composite-based NO_2 gas detection," *New Journal of Chemistry,* vol. 49, no. 42, pp. 18436-18446, 2025.

[6] S. H. S. Pai, R. Yeasmin, R. B. Ali, R. Samyugdhanayaki, G. Mohapatra, Q. A. Sial, A. S. Khan, and H. Seo, "Dual-platform chemochromic sensor for low concentration hydrogen gas detection using Y_2O_3/Pd nanocomposite-incorporated functional polymer: An experiment and DFT approach," *Sensors and Actuators B: Chemical,* vol. 450, p. 139230, 2025.

[7] Y. Shi, X. Li, X. Sun, X. Shao, and H. Wang, "Strategies for improving the sensing performance of In_2O_3-based gas sensors for ethanol detection," *Journal of Alloys and Compounds,* vol. 963, p. 171190, 2023.

[8] M. A. Belal, S. Hajra, S. Panda, K. R. Kaja, M. Magdy, A. A. E. Moneim, D. Janas, Y. K. Mishra, and H. J. Kim, "Advances in gas sensors using screen printing," *Journal of Materials Chemistry A,* vol. 13, no. 8, pp. 5447-5497, 2025.

[9] S. H. S. Pai, A. Mondal, B. Ajitha, and Y. A. K. Reddy, "Effect of calcination temperature on NiO for hydrogen gas sensor performance," *International Journal of Hydrogen Energy,* vol. 50, pp. 928-941, 2024.

[10] S. He, Y. Gui, Y. Wang, L. Cao, G. He, and C. Tang, "CuO/TiO_2/MXene-based sensor and SMS-TENG array integrated inspection robots for self-powered ethanol detection and alarm at room temperature," *ACS sensors,* vol. 9, no. 3, pp. 1188-1198, 2024.

[11] Z. H. Lin, G. Zhu, Y. S. Zhou, Y. Yang, P. Bai, J. Chen, and Z. L. Wang, "A self-powered triboelectric nanosensor for mercury ion detection," *Angewandte Chemie International Edition,* vol. 52, no. 19, 2013.

[12] Z. H. Lin, G. Cheng, L. Lin, S. Lee, and Z. L. Wang, "Water-solid surface contact electrification and its use for harvesting liquid-wave energy," *Angewandte Chemie,* vol. 125, no. 48, 2013.

[13] K. R. Kaja, S. Hajra, S. Panda, M. A. Belal, U. Pharino, H. Khanbareh, N. Vittayakorn, V. Vivekananthan, C. R. Bown, and H. J. Kim, "Exploring liquid-solid interface based tribo-electrification, structures, and applications," *Nano Energy,* vol. 131, p. 110319, 2024.

[14] R. Muddamalla, M. Navaneeth, A. A. Sharma, P. P. Pradhan, K. A. K. D. Prasad, U. K. Khanapuram, R. R. Kumar, and H. Divi, "Phosphor-based triboelectric nanogenerators for mechanical energy harvesting and self-powered systems," *ACS Applied Electronic Materials,* vol. 6, no. 3, pp. 1821-1828, 2024.

[15] S. Mishra, M. Rakshita, H. Divi, S. Potu, and R. K. Rajaboina, "Unique contact point modification technique for boosting the performance of a triboelectric nanogenerator and its application in road safety sensing and detection," *ACS Applied Materials & Interfaces,* vol. 15, no. 27, pp. 33095-33108, 2023.

[16] A. Panda, K. K. Das, K. R. Kaja, V. Gandi, S. G. Mohanty, and B. K. Panigrahi, "Low-cost high performance sustainable triboelectric nanogenerator based on laboratory waste," *Journal of Metals, Materials and Minerals,* vol. 35, no. 1, p. e2226, 2025.

[17] Z. Nan, G. Haojie, K. Lu, S. Ye, W. Xu, H. Zheng, Y. Song, C. Liu, J. Jiao, Z. Wang, and X. Zhou, "A universal single electrode droplet-based electricity generator (SE-DEG) for water kinetic energy harvesting," *Nano Energy,* vol. 82, p. 105735, 2021.

[18] U. Pharino, K. Chaithaweep, S. Pongampai, N. Chanlek, S. Kothan, J. Kaewkhoo, S. Hajra, H. J. Kim, W. Vittayakorn, S. Sriphan, and N. Vittayakorn, "A highly sensitive disease pre-screening approach for glycosuria: Triboelectric sensing at the liquid-solid interface," *Chemical Engineering Journal,* vol. 508, p. 160901, 2025.

[19] T. Charoonsuk, R. Muanghlua, S. Sriphan, S. Pongampai, and N. Vittayakorn, "Utilization of commodity thermoplastic poly-ethylene (PE) by enhanced sensing performance with liquid phase electrolyte for a flexible and transparent triboelectric tactile sensor," *Sustainable Materials and Technologies,* vol. 27, p. e00239, 2021.

[20] S. Panda, S. Hajra, Y. Oh, W. Oh, J. Lee, H. Shin, V. Vivekananthan, Y. Yang, Y. K. Mishra, and H. J. Kim, "Hybrid nanogenerators for ocean energy harvesting: Mechanisms, designs, and applications," *Small,* vol. 19, no. 25, p. 2300847, 2023.

[21] J. A. L. Jayarathna, and K. R. Kaja, "Energy-harvesting device based on lead-free perovskite," *AI, Computer Science and Robotics Technology,* vol. 3, no. 1, pp. 1-9, 2024.

[22] K. R. Kaja, S. Hajra, S. Panda, M. A. Belal. S. Nam, P. Pakawanit, B. K. Panigrahi, H. Khanbareh, C. R. Bowen, J. Yu, and H. J. Kim, "Waste polyethylene-coated fabrics for dual-mode interfaces triboelectrification for self-powered sensors," *Results in Engineering,* vol. 28, p. 107111, 2025.

[23] K. R. Kaja, S. Hajra, S. Panda, M. A. Belal. P. Pakawanit, N. Vittayakorn, C. R. Bowen, H. Khanbareh, and H. J. Kim, "Triboelectrification based on the waste waterproof textiles for multisource energy harvesting," *Advanced Sustainable Systems,* vol. 9, no. 5, p. 2400678, 2025.

[24] K. Chaithaweep, U. Pharino, S. Pongampai, S. Hajra, H. J. Kim, T. Charoonsuk, T. Maluangnont, S. Sriphan, and N. Vittayakorn, "High-performance droplet-based triboelectric nanogenerators: A comparison of device configuration and operating parameters," *Advanced Materials Technologies,* vol. 10, no. 9, p. 2401870, 2025.